Radiative decays of the 16.6 and 16.9 MeV states in ^{8}Be and tests of the conservation of the vector current in the $A = 8$ multiplet

L. De Braeckeleer, E. G. Adelberger, J. H. Gundlach, M. Kaplan,* D. Markoff, A. M. Nathan,†
W. Schieff, K. A. Snover, D. W. Storm, K. B. Swartz, and D. Wright
Department of Physics, FM-15, University of Washington, Seattle, Washington 98195

B. A. Brown
Department of Physics, Michigan State University, East Lansing, Michigan 48823
(Received 26 October 1994)

We measured the ^{4}He(α,γ) cross section at $\theta_\gamma = 90°$ across the 16.6 and 16.9 MeV resonances in ^{8}Be and obtained angular distributions on the peaks of both resonances. The decays of the 16 MeV doublet to the 3.0 MeV 2^+ final state have an (isovector $E2$)/(isovector $M1$) mixing ratio of (0.01 ± 0.03), an (isoscalar $E2$)/(isovector $M1$) mixing ratio of (0.21 ± 0.04), and an isovector $M1$ width of (2.80 ± 0.18) eV. Our result for the isovector $E2$ strength disagrees markedly with previous work. We observe ground-state $E2$ decays of both members of the doublet. We use our results, plus existing ^{8}Li and ^{8}B β-decay data, to test the conservation of the vector current and to constrain the second-class induced-tensor form factor. Finally, we compare our results to shell-model calculations.

PACS number(s): 24.80.−x, 23.20.Js, 27.20.+n

I. INTRODUCTION

Nuclear physics experiments have established the conservation of the vector current (CVC) to a precision of roughly 6% and the absence of second-class currents to a level $|g_{II}/g_A| < 0.7$ [1]. Both of these symmetries would presumably be exact in the limit of good isospin [2,3] but are broken by quark mass and charge differences. It is therefore of considerable interest to test these symmetries with sufficient precision to probe the level of expected isospin-violating effects [4]. Although the Ademollo-Gatto theorem [5] precludes linear isospin-breaking corrections to the weak-magnetism form factor, the u-d quark mass splitting will generate a spurious second-class induced-tensor current proportional to that mass difference [6–8].

The A=8 isotriplet, shown in Fig. 1 is well suited for testing CVC and for detecting a possible second-class induced-tensor form factor [9]. The CVC test compares the weak-magnetism (and possibly second-forbidden) vector form-factors extracted from the β-α angular correlations in the $2^+ \rightarrow 2^+$ beta decays of ^{8}Li and ^{8}B, to the isovector $M1$ (and possibly isovector $E2$) matrix elements for the isospin-analog γ-decays in ^{8}Be. This paper reports our study of the γ decays of the $J^\pi = 2^+$ analog state in ^{8}Be (actually an isospin-mixed doublet) using the ^{4}He(α,γ) reaction. The experiment is described in Sec. II. In Sec. III we discuss our experimental results and compare them to previous work. In Secs. IV and V we examine the consequences of our results for CVC and second-class current tests in the A=8 multiplet. In Sec. VI we compare the experimental data to shell-model calculations. Our conclusions are summarized in Sec. VII.

II. DESCRIPTION OF THE EXPERIMENT

A. Experimental strategy

We determined the $M1$ and $E2$ widths needed for the CVC test by measuring the ^{4}He(α,γ) cross section as a function of energy across the 16.6 and 16.9 MeV levels and obtaining photon angular distributions on the peaks of both resonances. Accurate measurements of the yields and angular distributions are made difficult by the photon and neutron backgrounds generated by the interaction of the beam with the windows of the ^{4}He target cell. All previous studies [10–13] used the same procedure to solve this problem. The helium gas was contained in a long cell, only the central part of which was seen by the detector; the extremities containing the entrance and the exit windows were shielded with lead. This technique effectively solved the background problem but led to several difficulties:

(1) To deduce the *absolute cross section*, the effective length of the gas cell as seen by the photon spectrometer (which differs significantly from the diameter of the collimator) must be determined either by a separate measurement or by Monte Carlo computation.

(2) To measure the photon *angular distribution*, different collimators must be used at each angle, and the angle-dependent spectrometer acceptance and effective cell length must be calculated. This potential source of systematic error is subtle because the different spectrom-

*Present address: Department of Radiology, University of Washington, Seattle, WA 98195.
†Permanent address: Department of Physics, University of Illinois, Urbana, IL 61801.

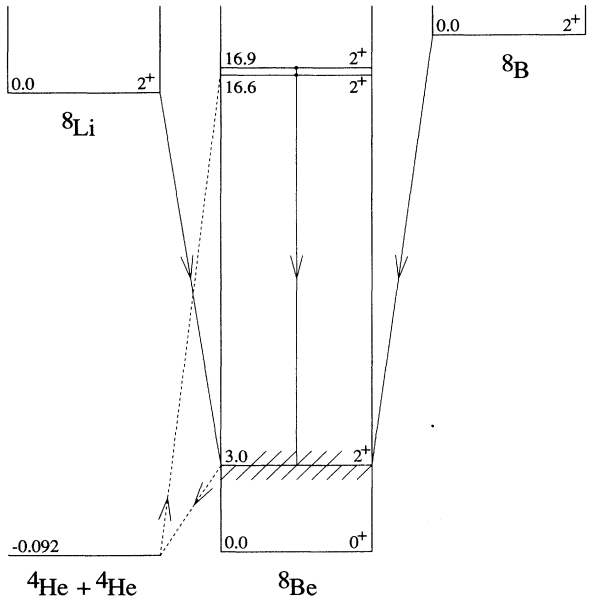

FIG. 1. Level diagram of the $A = 8$ isotriplet. The ^{8}Be isobaric analog of the ^{8}Li and ^{8}B ground states is split between the 16.6 and 16.9 MeV levels. In the CVC and second-class current tests, the isovector $M1$ decays of the ^{8}Be doublet to the broad 3.0 MeV level are compared to recoil-order effects in the analogous β decays of ^{8}Li and ^{8}B.

eter angles probe different regions of the gas cell and therefore different parts of the excitation function.

(3) Neutrons generated in the entrance window of a long gas cell may arrive in time with photons emitted from the central part of the cell so that the neutron background cannot be completely eliminated by time of flight. This prevented previous workers from taking data at forward angles, so they could not measure the purely kinematic forward-backward asymmetry that would have provided a check on the correctness and consistency of the angular distributions.

We solved the problems listed above by using an experimental setup (shown in Fig. 2) where a short, high-pressure cell with no collimation of the windows was bombarded by a pulsed α-particle beam. This technique left open the question of the background from the gas cell windows. This problem was solved by subtracting from the ^{4}He-target results background data taken with H_2 gas at a pressure that gave the same energy loss as when the cell was filled with helium. This insured that the beam energy at both the entrance and exit windows was the same in the 'full target' and 'background' runs and gave satisfactory subtractions as can be seen in Figs. 3 and 4.

B. The α-particle beam

The α-particle beams were provided by the University of Washington tandem-accelerator/superconducting-linac facility [14]. The beam had a time structure consisting of pulses of width <1 ns, at a repetition rate

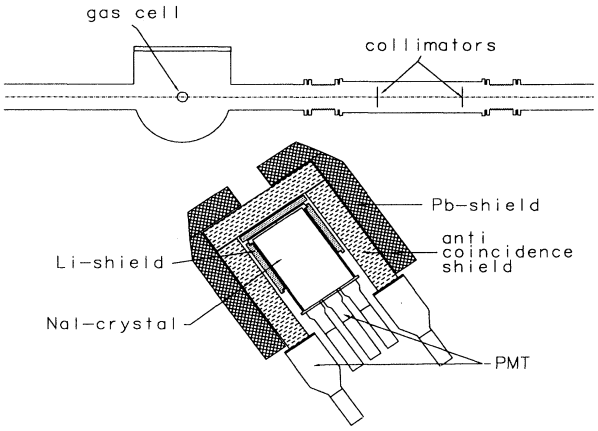

FIG. 2. Scale drawing of the detector and gas cell. A heavily shielded beam dump (not shown) was 7 m downstream from the target.

of 12.5 MHz, which allowed excellent rejection of the neutron background. It was clearly essential to control accurately the beam energy during the excitation function and angular distribution measurements. Because the linac beam did not pass through a conventional magnetic analysis system, it was necessary to have an independent monitor of the beam energy.

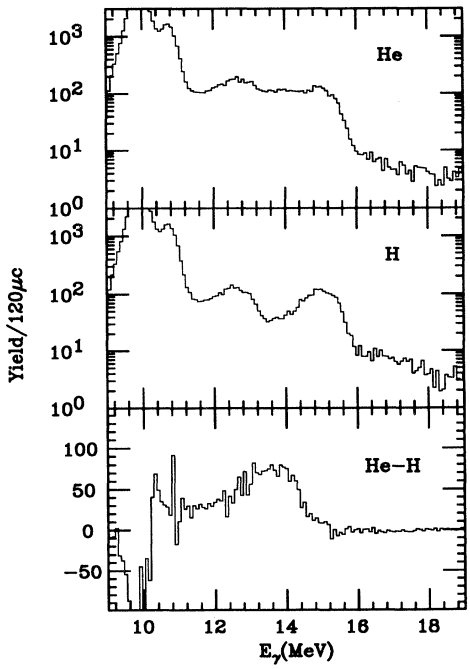

FIG. 3. Helium-filled target, hydrogen-filled target, and subtracted γ-ray spectra at $\theta_{lab} = 90°$, near the peak of the 16.9 MeV resonance. The prominent peaks at 12.7 and 15.1 MeV are Doppler-broadened γ rays from $^{12}C(\alpha, \alpha')$ reactions in the gas cell windows, while the 10.8 MeV peak is presumably due to $^{15}N(\alpha, \alpha')$ reactions in the Kapton windows. Counts below $E_\gamma = 10$ MeV were suppressed by an electronic threshold. The peak in the subtracted spectrum is from the ^{8}Be 16.9 $\rightarrow$ 3.0 decay.

Our beam-energy monitor consisted of two silicon counters, placed at (30 ± 1) degrees on the left and the right sides of the beam, that detected the α's elastically scattered by a 250 μg/cm^2 gold foil. The beam energy monitor was rotated into position and the pulse heights measured before and after any ^{4}He and H_2 run. The silicon counters were carefully calibrated even though we were mainly interested in determining relative energy shifts. The calibration of these detectors, based on ^{241}Am (E_α = 5.486 MeV) and ^{244}Cm (E_α = 5.805 MeV) sources, agreed with the predicted position of the resonance to within 40 keV out of 34 MeV. In anticipation of possible electronic shifts, low-energy and high-energy pulser signals were sent to both preamplifiers so that the origin of a shift (zero shift, gain shift, pulser drift, or beam-energy change) could be identified and, if spurious, corrected. Four energy shifts were observed in 120 measurements. Although these appeared to be gain shifts, the excitation curve data were not compatible with this hypothesis. The assumption of constant gain, on the other hand, produced good consistency of the excitation curve data (see Fig. 5), and this assumption was incorporated into the final analysis.

C. The gas cell

Our gas cell had a cylindrical geometry (4.45 cm diameter, 5.08 cm height) with 1.27 cm diameter holes for the entrance and exit windows. The axis of the cell was perpendicular to the beam axis and coincided (±2.5 mm) with the rotation axis of the photon spectrometer. For our application the most practical window materials were Kapton and nickel. A short measurement of the γ-ray background in the region of interest showed that Kapton windows were three times better than nickel, so we used the thinnest commercially available Kapton film (7.6 μm) as the window material.

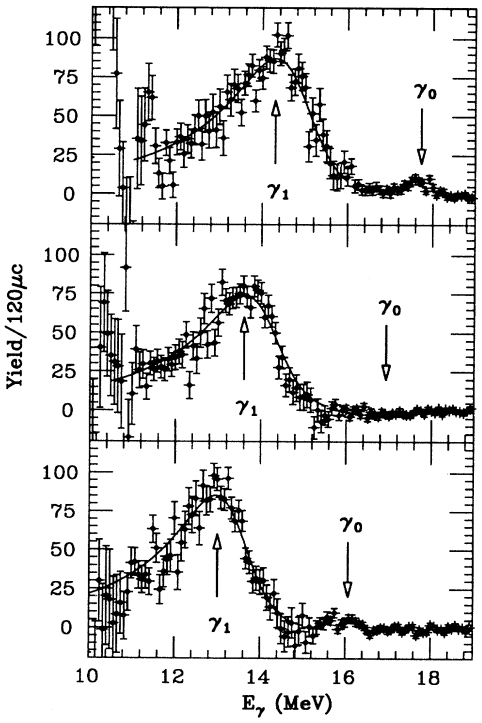

FIG. 4. Subtracted γ-ray spectra near the peak of the 16.9 MeV resonance. Top: θ_{lab} = 45°; middle: θ_{lab} = 90°; bottom: θ_{lab} = 140°. The 16.9 → 0.0 transition is clearly visible in the 45° and 140° spectra. The smooth curves show the best fit to the $2^+ \rightarrow 2^+$ transitions using the R-matrix final-state distribution which gave $M^\gamma_{16}/M^\gamma_3 = 1.6$. The curves are plotted in the spectral region that was fitted.

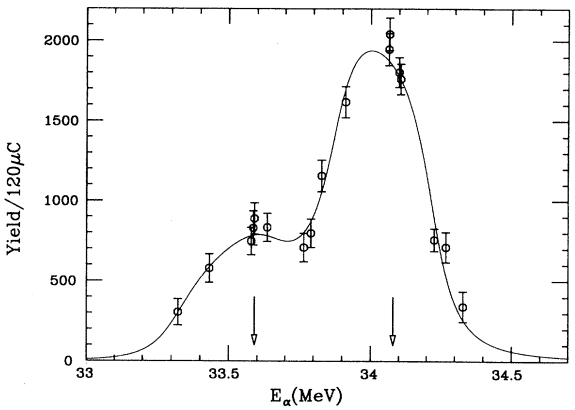

FIG. 5. ^{4}He(α,γ) excitation function at θ_{lab} = 90° for the decay to the 3 MeV level. Data were taken with a target thickness equivalent to ΔE_{lab} = 350 keV. The vertical arrows indicate the energies at which angular distributions were obtained. The curve is the best fit of the function given in Eq. (2) to the combined set of excitation function and angular distribution data.

Because we wanted to isolate the angular distributions of two closely spaced resonances (see Sec. IIA) while maintaining reasonable yields, we used a ^{4}He target thickness of 350 keV, corresponding to a helium pressure of ≈ 2 bar. Although this pressure was well below the 3 bar breaking point of the foils, radiation damage of the Kapton windows was a severe problem; windows typically failed after exposures of only 1 mC. For this reason the gas cell was equipped with three sets of windows equally spaced around the circumference of the cell. The gas cell was rotated to a new set of foils every 0.5 mC until all windows had been exposed, and then was replaced by a new gas cell. Nevertheless frequent failures occurred. The gas pressure was measured by a Baratron gauge and recorded continuously by an ADC. This procedure allowed us to monitor pressure drops, none of which exceeded 3%.

D. The NaI detector

Gamma rays were detected with the University of Washington large NaI spectrometer, consisting of a 25 cm by 38 cm central NaI scintillator enclosed successively in a ^{6}LiH shield, a 10-cm-thick plastic-scintillator anticoincidence counter, and a 10-cm-thick lead shield with a 15 cm cylindrical opening. The front face of the lead shield was 49.3 cm from the beam axis. This gave a flight path to the front face of the NaI crystal of approximately 80 cm, permitting good time-of-flight separation of neutrons and gammas over the entire angular range

45°–140° used in this work. The plastic anticoincidence threshold was set at a high level in order to maximize the detector efficiency without compromising the cosmic-ray rejection; with this arrangement the detector resolution was 6% at 15.1 MeV. The NaI gain was stabilized using a light-emitting-diode feedback system. The detector energy calibration was based on the positions of the 12.7 and 15.1 MeV $^{12}C(\alpha,\alpha')$ gamma rays produced in the Kapton foils. A 14.5 cm × 17 cm BaF_2 detector with a time resolution of <1 nsec continuously monitored the time structure of the beam. We used this detector to correct for small "satellite peaks" that were separated from the main peak by multiples of the 6.7 ns period of the linac RF. On average, this correction was 10%.

III. EXPERIMENTAL RESULTS

A. Expected form of the cross section

The ^{8}Be analog of the ^{8}Li and ^{8}B ground states is split into two levels by admixing with a nearby $T = 0$ level so that the physical 16.6 and 16.9 MeV states, $|a\rangle$ and $|b\rangle$, respectively, are related to the pure isospin states $|0\rangle$ and $|1\rangle$ by

$$|a\rangle = \alpha|1\rangle + \beta|0\rangle, \quad |b\rangle = \beta|1\rangle - \alpha|0\rangle \ . \tag{1}$$

The excitation energies and center-of-mass widths of the resonances, $E_a = 16.626$ MeV, $\Gamma_\alpha^a = 108.1$ keV, $E_b = 16.922$ MeV, and $\Gamma_\alpha^b = 74.0$ keV, are well determined from ^{4}He + ^{4}He scattering [15]. The magnitudes of the isospin-mixing parameters, $\alpha = 0.64$ and $\beta = -0.77$, are given by $\alpha^2/\beta^2 = \Gamma_\alpha^b/\Gamma_\alpha^a$, while the relative sign is fixed by the observed interference of the two resonances in the $^{10}B(d,\alpha)$ reaction [16].

A theoretical description of the $^4He(\alpha,\gamma)$ yield across the isospin-mixed 16.6 and 16.9 MeV resonances has been worked out by Barker [17], who finds

$$Y(E_x,\theta) = \frac{20\pi\lambda\!\!\!^{-2}}{S}\frac{Q}{Ze}\frac{\eta d\Omega}{4\pi}\alpha^2\beta^2\,\Gamma_{M1}^{T=1}\,\Gamma_\alpha \times \int_{E_x-\Delta/4}^{E_x+\Delta/4} \frac{|(E_b-E')[1+(\beta/\alpha)\epsilon]f_a^{1/2}(\theta) - (E_a-E')[1-(\alpha/\beta)\epsilon]f_b^{1/2}(\theta)|^2 dE'}{(E_a-E')^2(E_b-E')^2 + (\frac{1}{2}\Gamma_\alpha)^2(\alpha^2E_a+\beta^2E_b-E')^2} \ , \tag{2}$$

where $Y(E_x,\theta)$ is the center-of-mass yield at a mean excitation energy E and center-of-mass γ-ray angle θ. $S = 1.37\times10^{-15}$ eV cm^2/atom is the stopping power of the beam in ^{4}He gas, $\lambda\!\!\!^{-2} = 2\hbar^2/(m_\alpha E_\alpha)$, E_α is the laboratory energy of the beam in the center of the target, Δ is the energy loss of the beam in the target, Q and Z are the integrated charge and ionic state of the beam, and $\eta d\Omega/4\pi$ is the combined intrinsic and geometrical efficiency of the photon detector. $\Gamma_\alpha = \Gamma_\alpha^a + \Gamma_\alpha^b$, and $\Gamma_{M1}^{T=1}$ is the isovector $M1$ width in the center-of-mass frame. The isoscalar to isovector $M1$ ratio is $\epsilon = \left(\Gamma_{M1}^{T=0}/\Gamma_{M1}^{T=1}\right)^{1/2}$. The γ-ray widths are implicitly energy dependent; $\Gamma_{M1} \propto (E_\gamma/13.82\ \text{MeV})^3$ where 13.82 MeV is the mean E_γ of the isovector $M1$ gamma ray (see below).

It is worth noticing in Eq. (2) the implicit presence of a factor of 2 that accounts for the symmetrization in the incident channel but was omitted in previous works [10–13].

The angular distribution factors, $f_a(\theta)$ and $f_b(\theta)$, of the 16.6 and 16.9 MeV levels, are functions of the γ-ray multipolarities. The $2^+ \to 2^+$ transitions have the form

$$f_{a,b}(\theta) = a_0^{a,b} + a_2^{a,b}P_2(\cos\theta) + a_4^{a,b}P_4(\cos\theta) \ , \tag{3}$$

where

$$a_0^{a,b} = 1 + \delta_{a,b}^2 \ , \qquad a_2^{a,b} = 0.5 - 1.464\delta_{a,b} - 0.153\delta_{a,b}^2 \ ,$$

$$a_4^{a,b} = -0.491\delta_{a,b}^2 \ , \tag{4}$$

and $\delta_{a,b}$ is the $(E2/M1)$ amplitude mixing ratio of the γ ray originating from level a, b. The mixing ratios of the 16.6 and 16.9 MeV levels are related to the "isovector" and "isoscalar" mixing ratios, $\delta_1 = \left(\Gamma_{E2}^{T=1}/\Gamma_{M1}^{T=1}\right)^{1/2}$ and $\delta_0 = \left(\Gamma_{E2}^{T=0}/\Gamma_{M1}^{T=1}\right)^{1/2}$, by

$$\delta_a = \frac{\delta_1 + \delta_0\beta/\alpha}{1+\epsilon\beta/\alpha}, \qquad \delta_b = \frac{\delta_1 - \delta_0\alpha/\beta}{1-\epsilon\alpha/\beta} \ . \tag{5}$$

The laboratory angular distributions are related to those in the center-of-mass frame by

$$Y_{\rm lab}(E_x,\theta_{\rm lab}) = \frac{(1-\beta_{\rm c.m.}^2)}{(1-\beta_{\rm c.m.}\cos\theta_{\rm lab})^2}Y(E_x,\theta) \ , \tag{6}$$

with the center-of-mass velocity $\beta_{\rm c.m.} \approx 0.067$. It should be pointed out that this center-of-mass to laboratory transformation was done incorrectly in the previous measurement [12] of these angular distributions; the square in the denominator of Eq. (6) was omitted. The corresponding angle transformation is

$$\cos\theta = \frac{\cos\theta_{\rm lab} - \beta_{\rm c.m.}}{1-\beta_{\rm c.m.}\cos\theta_{\rm lab}} . \tag{7}$$

B. Experimental yields

Figure 4 shows typical $^4He(\alpha,\gamma)$ spectra from which we extracted the γ-ray yields. The yields are heavily

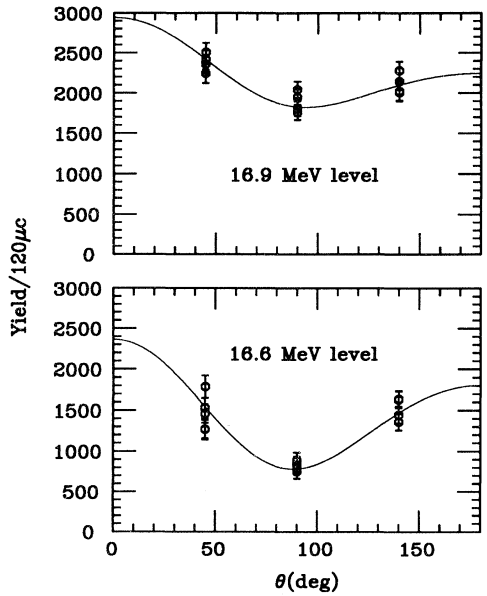

FIG. 6. Laboratory angular distributions of γ-ray transitions to the 3.0 MeV level. Top panel: near the peak of the 16.9 MeV resonance at $E_\alpha = 34.1$ MeV. Bottom panel: near the peak of the 16.6 MeV resonance at $E_\alpha = 33.6$ MeV. The curves are described in the caption of Fig. 5.

dominated by the $M1/E2$ transition to the broad 3 MeV 2^+ level of ^{8}Be. The $\theta_{\rm lab} = 90°$ excitation function for the $2^+ \rightarrow 2^+$ transition is shown in Fig. 5, and the angular distributions measured near the peaks of the 16.6 and 16.9 MeV resonances are shown in Fig. 6. The energy scales were calibrated using the Doppler-broadened 12.71 and 15.11 MeV ^{12}C(α,α') lines in the 90° hydrogen spectra. The data points in Figs. 5 and 6 were obtained by summing counts in a window that extended from $E_\gamma^{\rm c.m.} = E_\alpha^{\rm c.m.} - 5.08$ MeV to $E_\gamma^{\rm c.m.} = E_\alpha^{\rm c.m.} - 1.82$ MeV.

C. Analysis of the yields

Four unknown parameters can be determined from our data: $\Gamma_{M1}^{T=1}$, ϵ, δ_0, and δ_1. The shapes of the angular distribution are determined by δ_0 and δ_1, the shape of the excitation function (for fixed δ_0 and δ_1) is determined by ϵ, and the absolute scale of the yields is determined by $\Gamma_{M1}^{T=1}$. We fitted the combined data set–excitation function plus angular distributions, using Eqs. (2)–(7) with five free parameters: $\Gamma_{M1}^{T=1}$, ϵ, δ_0, and δ_1, plus ΔE, a constant that was added to E_α to account for the uncertainty in the absolute energy scale. The best fit, shown as the solid curves in Figs. 5 and 6, yields $\epsilon = +0.04 \pm 0.02$, $\delta_1 = +0.01 \pm 0.03$, and $\delta_0 = +0.21 \pm 0.04$. (The extraction of $\Gamma_{M1}^{T=1}$ is discussed in Sec. III D below.) The error bars in Figs. 5 and 6 reflect only the contribution from counting statistics. Additional fluctuating errors arose, for example, from small variations in the beam energy and from background subtraction uncertainties arising from time-dependent variation in the thicknesses of the Kapton foils. We accounted for these additional errors by inflating our uncertainties by a factor $\sqrt{\chi^2/\nu}$, where $\chi^2/\nu = 1.7$ is the chi-squared per degree of freedom computed assuming that counting statistics was the only source of error.

We disagree strongly with Bowles and Garvey [12], who found $\epsilon = -0.04 \pm 0.02$, $\delta_1 = +0.19 \pm 0.03$, and $\delta_0 = +0.22 \pm 0.03$. The discrepancy in δ_1 persists even when the data of Ref. [12] are reanalyzed using Eq. (6), yielding $\epsilon = -0.02 \pm 0.02$, $\delta_1 = 0.14 \pm 0.03$, and $\delta_0 = 0.26 \pm 0.04$. A reanalysis of the excitation function of Bowles and Garvey (see below), using our values of δ_1 and δ_0, yields $\epsilon = 0.00 \pm 0.03$. Note that although the extracted value of ϵ is very sensitive to the assumed isospin-mixing amplitudes, the quantity of primary interest for the CVC test, $\Gamma_{M1}^{T=1}$, is not; a 2% change in α would change our value for ϵ by 80%, while $\Gamma_{M1}^{T=1}$ would change by only 0.3%.

D. The isovector $M1$ width

Our absolute decay widths are based on a detector efficiency calibration obtained in a subsequent measurement of the well-known [18] ^{12}C$(p,\gamma)^{13}$N$(T = 3/2)$ resonance yield in the same geometry. Our empirical line shape, shown in Fig. 7, was constructed by appending the tail from a ^{11}B(p,γ) spectrum to the 15.1 MeV photopeak obtained from the on-resonance ^{12}C(p,γ) spectrum. The corresponding detection efficiency was $\eta\Delta\Omega/4\pi = (3.42 \pm 0.10) \times 10^{-3}$. Based on previous experience, we made the good approximation that the line shape depends only on the ratio E_d/E_γ, where E_d is the detected energy and E_γ is the γ-ray energy. A Monte Carlo calculation showed the efficiency to be flat in the 10–17 MeV range relevant to the present problem.

Because the ^{8}Be final state is very broad, it was necessary to account for its width in the data analysis. Studies [19,20] of ^{8}Li and ^{8}B β decays have shown that three $J^\pi = 2^+$ ^{8}Be levels must be included to account for

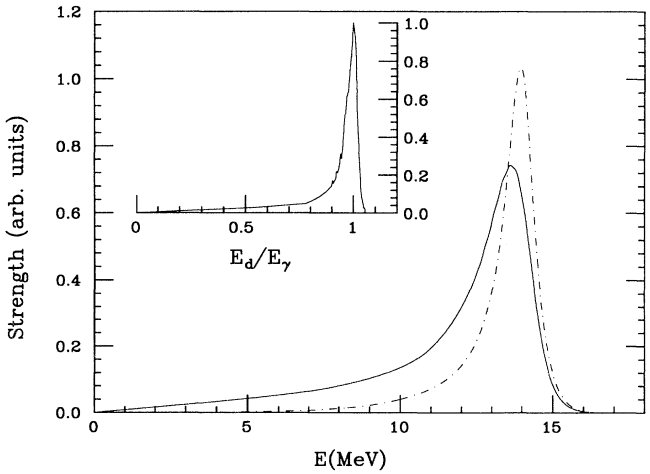

FIG. 7. The best-fit final-state distribution function for 16.9 $\rightarrow$ 3.0 dipole γ decay is shown as a dot-dashed line. The solid line shows the distribution function folded with the detector line shape. The line shape is displayed in the inset.

the observed shape of the final-state distribution. We parametrized the final-state shape using the R-matrix formalism as detailed, for example, in Ref. [19] and discussed further in Sec. IV below. We adopted a three-level description with states at $E_x \approx 3$ MeV, ≈ 16.6 MeV, and ≈ 16.9 MeV with $M1$ matrix elements M_1^γ, M_2^γ, and M_3^γ respectively. The R-matrix level energies and widths, shown in Table I, were fixed by other data. The values for the second and third levels were chosen to reproduce the known [15] physical energies and widths of the 16 MeV doublet, while the energy and width of the 3 MeV level were determined by fitting the α spectra [20] following ^{8}Li and ^{8}B β decays. Because our γ-ray spectra were not very sensitive to the details of the 16 MeV doublet, we made the simplifying assumption that a single $\Delta T = 1$ matrix element, M_{16}^γ, governed the transitions to the two 16 MeV levels. Therefore the shape of the γ-decay final-state function was determined by a single free parameter, $R_\gamma = M_{16}^\gamma / M_1^\gamma$, where M_1^γ is the matrix element for the transition to the 3 MeV level.

This single-parameter final-state distribution was folded with the detector lineshape as shown in Fig. 7 and fitted to the 45°, 90°, and 140° spectra shown in Fig. 4. The fit to these three spectra yielded $M_1^\gamma = 10.13 \pm 0.32$ and $R_\gamma = 1.6 \pm 1.8$ with $\chi^2/\nu = 1.31$. (The large uncertainty in R_γ confirms that our data have little sensitivity to contributions from the 16 MeV doublet.) These parameters imply a total $M1$ width of $\Gamma_{M1}^{T=1} = (2.80 \pm 0.18)$ eV, which is integrated over all final-state energies and quoted for an effective $T = 1$ initial-state excitation energy of $\overline{E}_x = \alpha^2 E_a + \beta^2 E_b = 16.80$ MeV corresponding to a mean γ-ray energy of 13.82 MeV. This width is dominated by decays to the 3 MeV level; decays to the 16 MeV level(s) make a very small contribution to the width because of the phase-space weighting factor. The 6.3% error quoted on $\Gamma_{M1}^{T=1}$ includes uncertainties from statistics (±3%), absolute efficiency (±3%), lineshape/efficiency extrapolation (±2%), stopping power (±2%), gas cell length due to foil bulge (±3%), and beam integration (±2%).

We compare our result to previous work by reanalyzing the excitation functions of Refs. [12] and [13], using the equations given in this work and our values of δ_a and δ_b. We extract $\Gamma_{M1}^{T=1} = (4.1 \pm 0.6)$ eV from the data of Paul *et al.* [13] which is considerably larger than our value. The same procedure applied to the Bowles and Garvey data [12] gives $\Gamma_{M1}^{T=1} = (3.6 \pm 0.3)$ eV, which is again larger than our value. In cases such as this, where some results may suffer from systematic error, it is not reasonable to try to extract a "best value" for $\Gamma_{M1}^{T=1}$ from the different experiments.

TABLE I. R-matrix parameters used in the analysis of ^{8}Be γ decays and ^{8}Li and ^{8}B β decays.

Quantity	Value
Radius (fm)	4.5
B_L	$S_L(E_1)$
E_1 (MeV)	3.20
γ_1 (MeV)$^{1/2}$	1.240
M_1^γ	10.13
M_1^β	0.1765[a]
E_2 (MeV)	16.626
γ_2 (MeV)$^{1/2}$	0.104
E_3 (MeV)	16.922
γ_3 (MeV)$^{1/2}$	0.0864
R_γ	1.6
R_β	−14.88

[a]This is the average of the ^{8}Li and ^{8}B values, which are 0.1818 and 0.1712, respectively.

E. The $E2$ ground-state transition

As is evident in Fig. 5, the ground-state decay of the 16.9 MeV level is clearly observed at 45° and 140° and is not seen at 90°, as expected for a $2^+ \to 0^+$ $E2$ transition. The angular distribution of counts in a narrow window centered on the photopeak is shown in the top panel of Fig. 8. The fitted curves shown in this figure have the form expected for a $2^+ \to 0^+$ transition: $Y(\theta) = A_0[1 + 0.714 P_2(\cos\theta) - 1.714 P_4(\cos\theta)]$. For the 16.9 MeV resonance, the fit yields $\Gamma_{E2}^{16.9} = (84 \pm 14)$ meV with $\chi^2/\nu = 2.5$. The ground-state transition from the 16.6 MeV resonance is seen clearly only at 45°; at this resonance, the fit is not as good ($\chi^2/\nu = 3.5$), and yields $\Gamma_{E2}^{16.6} = (70 \pm 25)$ meV, where the quoted errors again contain the factor $\sqrt{\chi^2/\nu}$ to account for sources of error other than counting statistics. (The relatively poor fit presumably arises because because Kapton foil thickness variations had a larger effect on the extraction of the yields such very weak transitions.) These widths correspond to reduced strengths $B(E2)_b = (0.075 \pm 0.013)\ e^2\text{fm}^4$ and $B(E2)_a = (0.068 \pm 0.024)\ e^2\text{fm}^4$. These reduced strengths can be decomposed into isoscalar and isovector components. Because the phases of the $E2$ matrix elements are unknown, there is a two fold ambiguity; either $B(E2)_{\rm IV} = (0.00 \pm 0.03)\ e^2\text{fm}^4$ and $B(E2)_{\rm IS} = (0.14 \pm 0.03)\ e^2\text{fm}^4$, or $B(E2)_{\rm IV} = (0.14 \pm 0.03)\ e^2\text{fm}^4$ and $B(E2)_{\rm IS} = (0.00 \pm 0.03)\ e^2\text{fm}^4$. Our results, together with $\Gamma_{M1}^{T=1}$ values from other work, are shown in Table II.

IV. A TEST OF CVC

We now use our results to test CVC in the $A = 8$ isotriplet. The laboratory-frame β-α correlations in ^{8}Li and ^{8}B decays have the general form

$$\omega(\theta_{\beta\alpha}, E_\beta, E_x) = F(Z, E_\beta) p_\beta E_\beta (E_0 - E_x - E_\beta)^2 \times [1 + a_1(E_\beta)\cos\theta_{\beta\alpha} + a_2(E_\beta)\cos^2\theta_{\beta\alpha}], \quad (8)$$

where F is the usual Fermi function, E_0 is the energy release for decays to the ^{8}Be ground state, and E_x is the excitation energy in ^{8}Be. The difference

$$\delta_{\rm exp}^-(E_\beta) = a_2(E_\beta;\ ^8\text{Li}) - a_2(E_\beta;\ ^8\text{B}) \quad (9)$$

is related to the weak form factors defined in Ref. [21] by

$$\delta^-(E_\beta)\frac{M}{E_\beta} = \frac{\int \left[b(E_x) - d_{\rm II}(E_x) - 3/\sqrt{14}f(E_x) - \sqrt{3/28}g(E_x)\frac{E_0-E_x-E_\beta}{M}\right] c(E_x)(E_0-E_x-E_\beta)^2 dE_x}{\int c^2(E_x)(E_0-E_x-E_\beta)^2 dE_x} , \quad (10)$$

where M is the nuclear mass, b is the weak-magnetism form factor, c is the Gamow-Teller form factor extracted from the ^{8}Li and ^{8}B lifetimes and β-delayed alpha spectra [19], $d_{\rm II}$ is a possible second-class form factor, and f and g are twice-forbidden vector form factors [22]. We account for the final-state distribution by allowing the form factors to be functions of E_x and integrating over E_x. Note that Eq. (10) assumes isospin symmetry of the Q values and matrix elements.

CVC relates the weak-magnetism form factor b to the isovector $M1$ width,

$$b(E_x) = M\sqrt{6\,\Gamma^{T=1}_{M1}(E_x)/(\alpha\,E_\gamma^3)} , \quad (11)$$

and predicts relations between f, g, and the isovector $E2/M1$ mixing ratio,

$$g = -\sqrt{2/3}\,\frac{2M}{E_0-E_x}f, \qquad f/b = \sqrt{10/3}\,\delta_1 . \quad (12)$$

As our value $\delta_1(E_x) = 0.01 \pm 0.03$ is consistent with zero [23] we neglect it in this analysis and obtain the CVC prediction,

$$\delta^-_{\rm CVC}(E_\beta)\frac{M}{E_\beta} = \frac{\int b(E_x)c(E_x)(E_0-E_x-E_\beta)^2 dE_x}{\int c^2(E_x)(E_0-E_x-E_\beta)^2 dE_x} , \quad (13)$$

where we have assumed that the second-class form factor is negligible. If only a single level were involved in the final state, b and c would be the same functions of E_x and this functional dependence would cancel in Eq. (13) so that $\delta^-_{\rm CVC}M/E_\beta$ would be independent of E_β. However, it has been observed in this work and in Refs. [10,12] that the *shape* of the final state in ^{8}Li and ^{8}B decays differs from that in the analogous γ decay of ^{8}Be indicating that c and b have different dependences on E_x. Prior to our work, there was no satisfactory explanation for this difference.

We employ a self-consistent analysis by parametrizing both $b(E_x)$ and $c(E_x)$ using a three-level R-matrix formalism with

$$b^2(E_x) \text{ or } c^2(E_x) = \frac{P_2(E_x)}{\pi}\,\frac{|\sum_{i=1}^3 \gamma_i M_i/(E_i-E_x)|^2}{|1-\{S_2(E_x)-B_2+iP_2(E_x)\}\{\sum_{i=1}^3 \gamma_i^2/(E_i-E_x)\}|^2} , \quad (14)$$

where the level parameters are listed in Table I, and S_2, P_2, and B_2 are the usual $L = 2$ R-matrix shift function, penetrability, and boundary condition, respectively. We assume that $M_2^{\beta,\gamma} = \alpha R_{\beta,\gamma} M_{16}^{\beta,\gamma}$ and $M_3^{\beta,\gamma} = \beta R_{\beta,\gamma} M_{16}^{\beta,\gamma}$, where the factors α and β are the isospin mixing amplitudes of the 16 MeV doublet. The Gamow-Teller matrix elements were extracted by fitting the high-

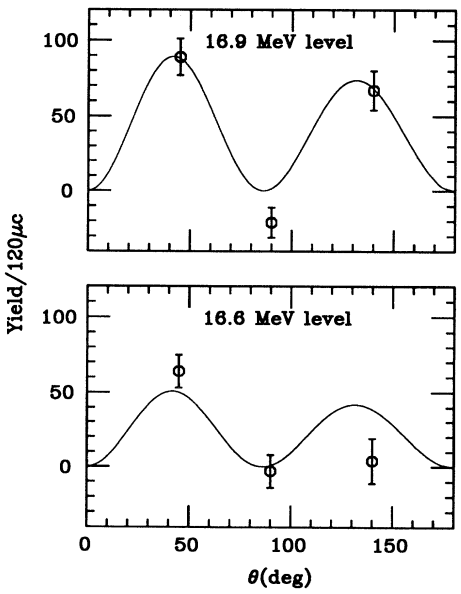

FIG. 8. Laboratory γ-ray angular distributions for decays to the ground state. Upper panel: 16.9 MeV resonance. Lower panel: 16.6 MeV resonance. The curves are fitted functions of the form expected for $2^+ \to 0^+$ decay.

TABLE II. Gamma decays of the 16 MeV 2^+ doublet in ^{8}Be. Entries are from this work, except where noted.

Final state	Observable	Value
2^+ (3.0 MeV)	$\Gamma^{T=1}_{M1}$	2.80 ± 0.18 eV [a]
		3.6 ± 0.3 eV [b]
		4.1 ± 0.6 eV [c]
2^+ (3.0 MeV)	ϵ	$+0.04 \pm 0.02$
2^+ (3.0 MeV)	δ_1	$+0.01 \pm 0.03$
2^+ (3.0 MeV)	δ_0	$+0.21 \pm 0.04$
0^+ (0.0 MeV)	$\Gamma_{E2}(16.6 \to 0.0)$	70 ± 25 meV
0^+ (0.0 MeV)	$\Gamma_{E2}(16.9 \to 0.0)$	84 ± 14 meV

[a]Quoted for $E_i = \overline{E} = 16.80$ MeV, the mean energy of the $2^+, T = 1$ strength, corresponding to $E_\gamma = 13.82$ MeV.
[b]From Bowles and Garvey [12] adjusted for our values of δ_1 and δ_0.
[c]From Paul *et al.* [13], adjusted for our values of δ_1 and δ_0.

TABLE III. Reduced transition strengths and mixing ratios for γ decays of the 16 MeV 2^+ doublet in ^{8}Be, and for the β decays of ^{8}Li and ^{8}B. Unless otherwise noted, experimental results and calculations are from this work. Our $B(GT)$ values contain the $(g_A/g_V)^2$ factor. The $E2$ calculations use effective charges of $e_p = 1.35e$ and $e_n = 0.35e$ that reproduce the strong $2^+ \rightarrow 0^+$ transition of the ground-state band.

Final state	Observable[a]	CKI[b]	Kumar[c]	CKPOT[d]	van Hees[e]	Expt.
2^+ (3.0 MeV)	$B(M1, IV)$	0.18	0.17	0.37	0.52	0.091 ± 0.006
2^+ (3.0 MeV)	$B(M1, IS)$	$(5.4)10^{-4}$	$(2.1)10^{-4}$	$(12)10^{-4}$	$(18)10^{-4}$	$(2 \pm 2)10^{-4}$
2^+ (3.0 MeV)	ϵ	-0.054	-0.035	-0.058	-0.059	$+0.06 \pm 0.02$
2^+ (3.0 MeV)	$B(GT)$	0.035	0.044	0.105	0.143	0.031
2^+ (3.0 MeV)	$B(E2, IV)$	$(3.1)10^{-3}$	$(5.4)10^{-3}$	$(2.7)10^{-3}$	$(2.3)10^{-3}$	$(1 \pm 6)10^{-3}$
2^+ (3.0 MeV)	$B(E2, IS)$	0.19	0.069	0.60	0.85	0.30 ± 0.12
0^+ (0.0 MeV)	$B(E2, IV)$	0.071	0.046	0.094	0.144	0.00 ± 0.03 or 0.14 ± 0.03
0^+ (0.0 MeV)	$B(E2, IS)$	0.034	0.000	0.047	0.060	0.14 ± 0.03 or 0.00 ± 0.03
2^+ (3.0 MeV)	δ_1	$+0.015$	-0.021	$+0.010$	$+0.008$	$+0.01 \pm 0.03$
2^+ (3.0 MeV)	δ_0	$+0.12$	$+0.074$	$+0.15$	$+0.15$	$+0.22 \pm 0.04$
	R_β[f]	-10.3	-7.8	-6.2	-5.0	-14.88 ± 0.12
	$R_\gamma(T = 1 \rightarrow T = 0)$[f]	-6.2	-5.5	-4.6	-3.6	$+1.6 \pm 1.8$
	$R_\gamma(T = 1 \rightarrow T = 1)$	-1.8	-1.9	-1.3	$-1.1xx$	
	$R_\gamma(T = 0 \rightarrow T = 0)$	-2.0	-2.1	-1.3	-1.1	

[a] $B(M1)$ in units of μ_N^2 and $B(E2)$ in units of $e^2\text{fm}^4$.
[b] 6-16 TBME interaction of Ref. [27].
[c] Reference [28].
[d] CKPOT interaction from Ref. [27].
[e] Reference [29].
[f] Defined in the text.

statistics shapes [19,20] of the α spectra in ^{8}Li and ^{8}B decay, while the $M1$ matrix elements were extracted by fitting our γ spectra as described above. The β-decay matrix-element ratio $R_\beta = M_{16}^\beta / M_1^\beta = -14.88 \pm 0.12$, differs substantially from the corresponding ratio, $R_\gamma = 1.6 \pm 1.8$, observed in the γ decays. This difference, which can arise because the l term in the $M1$ operator has no analog in the Gamow-Teller operator, is responsible for the different shapes of $b(E_x)$ and $c(E_x)$. These shapes, computed from the parameters given in Table I, are shown in Figs. 9 and 10.

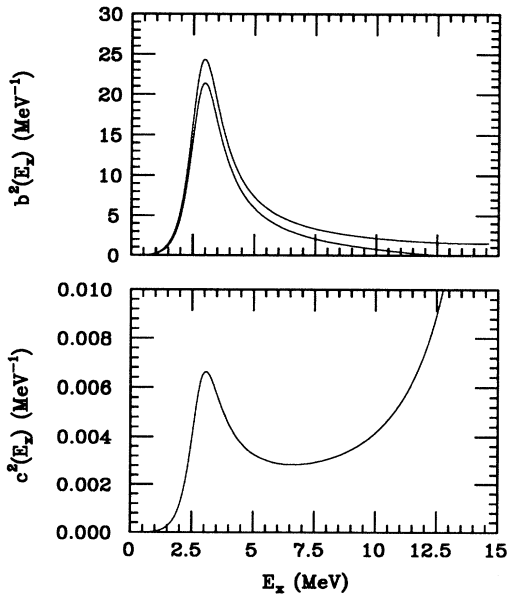

FIG. 9. Squares of form factors used in our CVC analysis. The upper panel shows $b^2(E_x)$ where the 1σ error band reflects our uncertainties in $\Gamma_{M1}^{T=1}$ and δ_1. The lower panel shows $c^2(E_x)$ inferred from the β-delayed α spectra from ^{8}Li and ^{8}B decay; the 1σ error band lies within the width of the line. The difference between these two form factors arises because of the complex final state and the different forms of the $M1$ and GT operators.

Figure 11 compares our CVC prediction, $\delta_{\text{CVC}}^-(E_\beta)$, to the measurements of Tribble and Garvey [24] and of McKeown, Garvey and Gagliardi [25]. We quantify this CVC test by scaling the predicted $\delta_{\text{CVC}}^-(E_\beta)$ from Eq. (13) by a factor κ and finding the value of κ that gives the best fit to the data shown in Fig. 11. The data of Tribble and Garvey yield

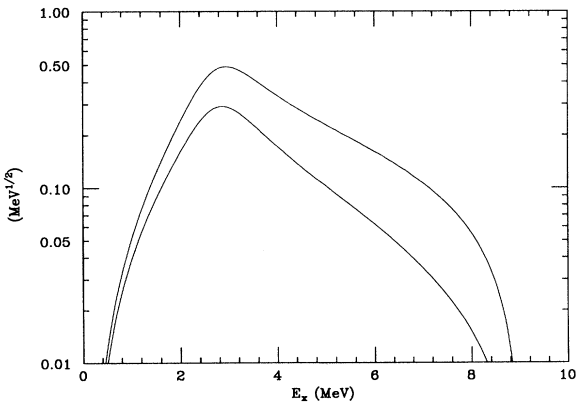

FIG. 10. Factors appearing in the integrands of Eq. (13). The upper curve shows $c(E_x)|E_0 - E_x - E_\beta|$, while the lower curve displays $100 \times b(E_x)|E_0 - E_x - E_\beta|$, both for a typical value of $E_\beta = 8$ MeV. Note that excitation energies above 6 MeV play a very small role in the δ_{CVC}^- prediction.

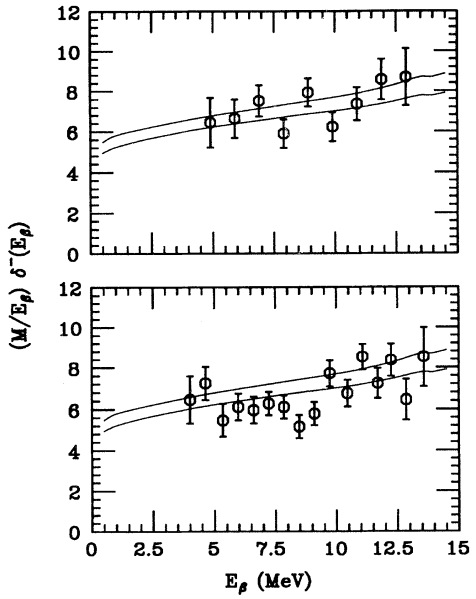

FIG. 11. The ^{8}Li-^{8}B β-α asymmetry factor $(M/E_\beta)\delta^-$ versus E_β. The smooth curves are our CVC prediction, with the $\pm 1\sigma$ error bands from our experimental uncertainties in $\Gamma_{M1}^{T=1}$, δ_1, and R_γ. The data points in the upper panel are measured values from Ref. [24]; those in the lower panel are from Ref. [25].

$$\kappa = \frac{\delta^-_{\rm exp}}{\delta^-_{\rm CVC}} = 1.00 \pm 0.04 \pm 0.05 \ , \tag{15}$$

with $\chi^2/\nu = 0.96$, while the data of McKeown, Gagliardi, and Garvey yield

$$\kappa = \frac{\delta^-_{\rm exp}}{\delta^-_{\rm CVC}} = 0.93 \pm 0.03 \pm 0.05 \ , \tag{16}$$

with $\chi^2/\nu = 1.64$. In both cases the first error reflects the quality of the fit and is inflated by $\sqrt{\chi^2/\nu}$, while the second error reflects the 3% scale-factor uncertainty in b from the error in $\Gamma_{M1}^{T=1}$, and the $\approx 3\%$ shape uncertainty in b arising from the errors in δ_1 and R_γ.

V. LIMITS ON SECOND-CLASS CURRENTS

If we assume the validity of CVC, our experiment together with the β-α correlation results from Refs. [24] or [25] can be used to limit the second-class induced-tensor form factor in the $A = 8$ isotriplet. In the impulse approximation $d_{\rm II}$ involves the same operator as c, so that $d_{\rm II}/c$ is independent of E_x. Then Eq. (10) becomes

$$\delta^-_{\rm exp}(E_\beta) = \delta^-_{\rm CVC}(E_\beta) + \frac{E_\beta}{m_N}\frac{d_{II}}{Ac} \ , \tag{17}$$

where we have set $M = Am_N$. Using the β-α correlation data of Ref. [24] plus the results of Eq. (17) we obtain a limit

$$\frac{d_{\rm II}}{Ac} = 0.0 \pm 0.3 \pm 0.3 \ , \tag{18}$$

with $\chi^2/\nu = 0.96$, while the data of Ref. [25] yield the limit

$$\frac{d_{\rm II}}{Ac} = -0.5 \pm 0.2 \pm 0.3 \ , \tag{19}$$

with $\chi^2/\nu = 1.62$. The errors are computed as for the CVC tests discussed above.

VI. COMPARISON TO SHELL-MODEL PREDICTIONS

Although our CVC and second-class current tests are independent of any specific nuclear models, the γ and β-decay data do provide useful constraints on structure calculations. In this section we compare the data to several shell model calculations.

The dominant configurations of the ground state, the 3.0 MeV level, and the 16 MeV doublet (along with the ^{8}Li and ^{8}B ground states) are $[4]^1$S, $[4]^1$D, and $[31]^3$P, respectively. Therefore decays of the 16 MeV levels (and of ^{8}Li and ^{8}B) to the low-lying states of ^{8}Be are expected to be suppressed. $E2$ decays are suppressed because the $E2$ operator cannot change S, GT β decay to the 3 MeV level is suppressed because the operator cannot change the spatial symmetry, and $M1$ decay to the 3 MeV level is inhibited because only the $l\tau$ term in the operator can contribute (the σ and $\sigma\tau$ terms cannot change the spatial symmetry and the l term cannot change L). These expectations are qualitatively consistent with the experimental reduced $M1$, $E2$, and GT strengths for $2^+ \rightarrow 2_1^+$ transitions. All of these are significantly retarded: $B(M1)_{\rm IV} = 0.05$ W.u., $B(E2)_{\rm IS} = 0.3$ W.u., and $B(GT) = 0.031$ [26]. In contrast, the β and γ decays to the 16 MeV levels are expected to be strong, in qualitative accord with the data.

Table III shows the reduced γ- and β-decay transition strengths and mixing ratios calculated using the $1p$-shell wave functions of Cohen and Kurath [27], Kumar [28] and van Hees [29]. The signs of ϵ and δ_0 are normally arbitrary in shell model calculations, because the $T = 0$ and $T = 1$ components of the unmixed doublet are independent eigenstates. We calculated the signs of ϵ and δ_0 by computing isospin-mixing amplitudes for the doublet and comparing the signs of these amplitudes to the empirical values of α and β. The relative signs of the γ-(or β decay) amplitudes feeding the 3 MeV and 16 MeV final states were predicted by calculating both the γ-decay (or β-decay) matrix elements and the α-formation (or α-decay) matrix elements using the same wave functions so that the arbitrary signs entered twice and therefore cancelled.

The best calculations (CKI and Kumar) of the relatively weak $2^+ \rightarrow 2_1^+$ $M1$ isovector strength overpredict the experimental value by a factor of 2. The $2^+ \rightarrow 2^+$ (isoscalar $M1$)/(isovector $M1$) matrix-element ratio ϵ is small both experimentally and theoretically; however the measured and calculated signs disagree. The

CKI and Kumar calculations predict a GT strength to the 2_1^+ level that is slightly larger than than the observed value.

On the other hand, the $M1$ and GT transitions to the tails of 16 MeV levels are predicted to have substantial reduced strengths, with $B(GT)$'s and $B(M1)$'s values ranging from about 3 to about 7. All calculations give the correct sign for R_β, and the CKI interaction shows reasonable agreement with the magnitude. The situation for R_γ is less satisfactory; all calculations overpredict this quantity.

All calculations correctly predict that the $2^+ \rightarrow 2^+$ $E2$ transition is predominantly isoscalar; i.e., that δ_1 is much smaller than δ_0, and also give the correct sign for δ_0. In contrast, the $2^+ \rightarrow 0^+$ $E2$ decays are predicted to be predominantly isovector, which agrees with one of the two possible solutions for the experimental decomposition of this strength, as shown in Table III. It differs, however, from the predictions of the Alaga rule [30] which requires the $2^+ \rightarrow 2^+$ and $2^+ \rightarrow 0^+$ transitions to have the same isospin character, and their intensities to be in the ratio [31]

$$\frac{B(E2;\, 2^+ \rightarrow 2^+)}{B(E2;\, 2^+ \rightarrow 0^+)} = \frac{10}{7} = 1.43 \ . \tag{20}$$

These predictions are in accord with the other experimentally allowed solution, which yields

$$\frac{B(E2;\, 2^+ \rightarrow 2^+)}{B(E2;\, 2^+ \rightarrow 0^+)} = 2.1 \pm 1.0 \ . \tag{21}$$

The shell-model calculations deviate from the Alaga rule because of SU(3) symmetry breaking for these weak $E2$ transitions.

Overall, our experimental results are in reasonable agreement with the range of values predicted by the calculations. In particular, the much smaller value for $B(E2,\mathrm{IV},16 \rightarrow 3)$ obtained in this work compared to the previous experiment brings this quantity into agreement with theoretical expectations. Furthermore, our explanation of the differences in the final-state distributions given in our discussion of the CVC and SCC tests above is also in qualitative accord with the best shell-model calulations.

VII. CONCLUSIONS

Our results alter substantially the details of the CVC and second-class current tests in the $A = 8$ isotriplet. Both our isovector $E2/M1$ mixing ratio δ_1 and our isovector $M1$ radiative width $\Gamma_{M1}^{T=1}$ are significantly smaller than the values found previously. Our smaller isovector $E2$ strength is now in accord with shell-model expectations, while the previous large value was hard to explain. The smaller $E2$ strength will make it quite difficult to use the $A = 8$ nuclei for a precise test of CVC in quadrupole order as had been proposed previously [1]. The changes in $\Gamma_{M1}^{T=1}$ and δ_1 tend to compensate in the dipole-order CVC test so that we find no evidence for CVC violation, a conclusion that is consistent with previous work but for rather different reasons.

We are now preparing a new experiment to measure the $^4\mathrm{He}(\alpha,\gamma)$ excitation function and γ-ray spectrum shape. In addition we are measuring the β-α correlations in ^{8}Li and ^{8}B decays. These results should lead to CVC and second-class current tests with improved sensitivities.

ACKNOWLEDGMENTS

We are grateful to F. C. Barker for theoretical advice. This work was supported in part by the U.S. Department of Energy. A.M.N. and B.A.B. acknowledge support from NSF Grants 89-21146 and 94-03666, respectively.

[1] L. Grenacs, Annu. Rev. Nucl. Part. Sci. **35**, 455 (1985).
[2] E. Commins and P. Bucksbaum, *Weak Interactions of Leptons and Quarks* (Cambridge University Press, Cambridge, England, 1983).
[3] E. Henley and L. Wolfenstein, Phys. Lett. **36B**, 28 (1976).
[4] *A Long Range Plan for Nuclear Science*, a report by the DOE-NSF Nuclear Science Advisory Committee, 1983, pp. 25–27.
[5] M. Ademollo and R. Gatto, Phys. Lett. **13**, 264 (1964).
[6] A. Halprin, B. W. Lee, and P. Sorba, Phys. Rev. D **14**, 2343 (1976).
[7] J. F. Donoghue and B. R. Holstein, Phys. Rev. D **25**, 206 (1982).
[8] B. M. K. Nefkens, G. A. Miller, and I. Šlaus, Comments Nucl. Part. Phys. **20**, 221 (1992).
[9] L. De Braeckeleer, Phys. Rev. C **45**, 1935 (1992).
[10] A. M. Nathan, Ph. D. thesis, Princeton University, 1975.
[11] A. M. Nathan, G. T. Garvey, P. Paul, and E. K. Warburton, Phys. Rev. Lett. **35**, 1137 (1975).
[12] T. J. Bowles and G. T. Garvey, Phys. Rev. C **18**, 1447 (1978); **26**, 2336 (1982); T. J. Bowles, Ph.D. thesis, Princeton University, 1977.
[13] P. Paul, M. Suffert, and Ph. Gorodetzky, Phys. Lett. **71B**, 71 (1977).
[14] D. W. Storm, J. F. Amsbaugh, D. T. Corcoran, G. C. Harper, M. A. Howe, R. E. Stowell, W. G. Weitkamp, T. D. Van Wechel, and D. J. Will, Nucl. Instrum. Methods **A287**, 247 (1990).
[15] See results summarized by F. Ajzenberg-Selove, Nucl. Phys. **A490**, 1 (1988).
[16] W. D. Callendar and C. P. Browne, Phys. Rev. C **2**, 1 (1970).
[17] F. C. Barker, Austral. J. Phys. **20**, 341 (1967).
[18] R. E. Marrs, E. G. Adelberger, and K. A. Snover, Phys. Rev. **C16**, 61 (1977).
[19] E. K. Warburton, Phys. Rev. C **33**, 303 (1986).
[20] L. De Braeckeleer and D. Wright, unpublished data.
[21] B. R. Holstein, Rev. Mod. Phys. **46**, 789 (1974).
[22] This expression is correct to first order in the induced currents.
[23] If, in the future, a nonzero δ_1 were to be obtained from a more accurate experiment, the energy dependence of $\delta_1(E_x)$ would be needed to make a model-independent

test of CVC.
[24] R. E. Tribble and G. T. Garvey, Phys. Rev. C **12**, 967 (1975).
[25] R. D. McKeown, G. T. Garvey, and C. A. Gagliardi, Phys. Rev. C **22**, 738 (1980).
[26] This $B(GT)$ was obtained by fitting the data of Ref. [20]; it also reproduces the spectra in Ref. [19]. Our value disagrees with that quoted by W. T. Chou, E. K. Warburton, and B. A. Brown, Phys. Rev. C **47**, 163 (1993). This difference could be explained if the matrix element quoted in Ref. [19] is in units of g_A/g_V.
[27] S. Cohen and D. Kurath, Nucl. Phys. **73**, 1 (1965).
[28] N. Kumar, Nucl. Phys. **A225**, 221 (1974).
[29] A. G. M. van Hees, A. A. Wolters, and P. W. M. Glaudemans, Nucl. Phys. **A476**, 61 (1988).
[30] J. M. Eisenberg and W. Greiner, *Nuclear Models* (American Elsevier, New York, 1970).
[31] This assumes that the doublet levels have $K = 2$ and that the ground and 3 MeV levels are members of a $K = 0$ band.